2000

# Parallel climate model (PCM) control and transient simulations

Semtner, A.J. Jr.

Springer-Verlag

Climate Dynamics (2000) 16:755-774
http://hdl.handle.net/10945/48927

Climate Dynamics (2000) 16:755–774 

**W. M. Washington · J. W. Weatherly**
**G. A. Meehl · A. J. Semtner Jr. · T. W. Bettge**
**A. P. Craig · W. G. Strand Jr. · J. Arblaster**
**V. B. Wayland · R. James · Y. Zhang**

# Parallel climate model (PCM) control and transient simulations

Received: 19 August 1999 / Accepted: 29 February 2000

**Abstract** The Department of Energy (DOE) supported Parallel Climate Model (PCM) makes use of the NCAR Community Climate Model (CCM3) and Land Surface Model (LSM) for the atmospheric and land surface components, respectively, the DOE Los Alamos National Laboratory Parallel Ocean Program (POP) for the ocean component, and the Naval Postgraduate School sea-ice model. The PCM executes on several distributed and shared memory computer systems. The coupling method is similar to that used in the NCAR Climate System Model (CSM) in that a flux coupler ties the components together, with interpolations between the different grids of the component models. Flux adjustments are not used in the PCM. The ocean component has 2/3° average horizontal grid spacing with 32 vertical levels and a free surface that allows calculation of sea level changes. Near the equator, the grid spacing is approximately 1/2° in latitude to better capture the ocean equatorial dynamics. The North Pole is rotated over northern North America thus producing resolution smaller than 2/3° in the North Atlantic where the sinking part of the world conveyor circulation largely takes place. Because this ocean model component does not have a computational point at the North Pole, the Arctic Ocean circulation systems are more realistic and similar to the observed. The elastic viscous plastic sea ice model has a grid spacing of 27 km to represent small-scale features such as ice transport through the Canadian Archipelago and the East Greenland current region. Results from a 300 year present-day coupled climate control simulation are presented, as well as for a transient 1% per year compound $CO_2$ increase experiment which shows a global warming of 1.27 °C for a 10 year average at the doubling point of $CO_2$ and 2.89 °C at the quadrupling point. There is a gradual warming beyond the doubling and quadrupling points with $CO_2$ held constant. Globally averaged sea level rise at the time of $CO_2$ doubling is approximately 7 cm and at the time of quadrupling it is 23 cm. Some of the regional sea level changes are larger and reflect the adjustments in the temperature, salinity, internal ocean dynamics, surface heat flux, and wind stress on the ocean. A 0.5% per year $CO_2$ increase experiment also was performed showing a global warming of 1.5 °C around the time of $CO_2$ doubling and a similar warming pattern to the 1% $CO_2$ per year increase experiment. El Niño and La Niña events in the tropical Pacific show approximately the observed frequency distribution and amplitude, which leads to near observed levels of variability on interannual time scales.

W. M. Washington (✉) · G. A. Meehl · T. W. Bettge
A. P. Craig · W. G. Strand Jr. · J. Arblaster · V. B. Wayland
R. James
National Center for Atmospheric Research (NCAR),
1850 Table Mesa Drive, Boulder, CO 80307, USA
E-mail: wmw@ucar.edu

J. W. Weatherly
US Army Cold Regions Research and Engineering
Laboratory (CRREL), USA

A. J. Semtner Jr. · Y. Zhang
US Naval Postgraduate School (NPS), USA

## 1 Introduction

The main purpose is to describe results from the Department of Energy (DOE) supported Parallel Climate Model (PCM) for a 300 year present-day climate control run without flux adjustment, a 0.5% per year $CO_2$ increase experiment to the time of $CO_2$ doubling, and a 1% per year $CO_2$ increase experiment with idealized stabilization at doubling and quadrupling of $CO_2$. The DOE PCM has substantially higher resolution in the ocean and sea-ice components compared to most coupled climate models. Among the difficulties in earlier climate change simulations is that some of the features in the climate models were of low resolution and the treatment of many of the physical processes was quite simple. The PCM components are of higher

resolution and the physical processes are more realistic. It is clear that climate models have substantially improved over the last decade, however, there are still shortcomings. Because of the higher resolution in the climate change simulations shown here, we are better able to investigate regional ocean and sea-ice changes. Also, the use of increased horizontal equatorial ocean resolution and low values of vertical mixing coefficients contributes to a higher amplitude El Niño-La Niña cycle than in previous versions, which in turn increases the interannual tropical climate variability (Meehl et al. 2000b). This is especially relevant to the large-scale forcing of the Pacific Sea surface temperature anomalies and their effect on the extratropical planetary waves.

A second purpose is to briefly describe how the PCM is implemented on new generation parallel processor computers. The DOE Computer Hardware, Advanced Mathematics and Model Physics (CHAMMP) Program and the DOE Climate Change Prediction Program (CCPP) have, for many years, addressed improvements in next-generation climate models. Two of the novel aspects are that the components used have been developed at distributed research centers, and they are all designed for parallel processor (typically non-vector) supercomputers. The PCM can be run either on clusters of shared-memory multi-processor (SMP) computers or distributed memory (DM) computers, which are both increasing in use at climate modeling research centers. NCAR also has developed the Climate System Model (CSM), which is mostly National Science Foundation (NSF) supported with extensive involvement of the academic community. The CSM and PCM are complementary and use some of the same overall concepts (and the same atmospheric component) except the PCM uses a parallel computer technique and different ocean and sea-ice components, which are of higher resolution. Recently, the DOE has developed an Accelerated Climate Prediction Initiative (ACPI) in which it is planned to have computer capacity in the year 2003 up to many Tera-operations per second with large numbers of processors. The PCM specifically has developed a modeling strategy that will use such computer capacity. Semtner (2000) has published a review article on ocean and climate modeling for advanced parallel computers that describes the potential advances in this area.

## 2 Atmospheric/land component

The atmospheric component is the parallel version of the NCAR Community Climate Model version 3 (CCM3) at T42 horizontal resolution and 18 hybrid levels in the vertical. This model includes the latest published versions of radiation, boundary-layer physics, and precipitation physics. The CCM3 is described in detail in Kiehl et al. (1998), Hack et al. (1998), Hurrell et al. (1998), and Briegleb and Bromwich (1998). The CCM has evolved from earlier versions. This version is a spectral model for the basic dynamics and uses a T42 resolution, which is about 2.9° in latitude and longitude. Penetrative convection is parametrized by the method of Zhang and McFarlane (1995) and the Hack (1994) scheme is used for shallow convection. The cloud fraction and optical properties are computed diagnostically from grid scale parameters including the convection variables as described in Kiehl et al. (1998). The boundary layer turbulent fluxes of momentum, heat and moisture are computed using the method of Holtslag and Boville (1993). The longwave radiation takes into account $CO_2$, $O_3$, $H_2O$, $CH_4$, $N_2O$, CFC11, CFC12 all of which are greenhouse gases. In order to achieve a balance of fluxes at the top of the atmosphere, small adjustments are made to the cloud parameters to achieve energy balance in the case of specified ocean sea surface temperatures. Bonan (1996) has developed the land-surface model (LSM) part of CCM3. It is a one-dimensional model of the energy, momentum, and water exchanges between the atmosphere and earth's surface. The LSM takes into account prescribed vegetation types, hydraulic and thermal properties of prescribed soil types. It also considers multiple surface types including lakes and wetlands within an atmospheric grid cell. There are twelve different soil types and 28 different surface types included in the formulation. Hack et al. (1995) incorporated a parallel partitioning strategy for the CCM3 with one-dimensional decomposition along latitude circles, which provides an efficient implementation on parallel computers. This decomposition method is effective for triangular spectral truncation at 42 wave numbers (T42) with 64 processors. However, this version of CCM3 does not scale well beyond 64 processors at T42 resolution. The use of such techniques in making a more scalable version of an atmospheric model has been implemented at a number of centers such as the European Centre for Medium Range Weather Forecasts (ECMWF) and the UK Hadley Centre. There is an ongoing collaborative effort between Oak Ridge National Laboratory, Argonne National Laboratory and NCAR to incorporate the CCM3 physical processes into a more scalable version of CCM. Adding this feature should allow for a large number of processors to be used on the PCM and should make the PCM more linearly scaleable to a large number of processors in the range of 100 to 200 depending upon which parallel computer system is being used.

## 3 Ocean component

The PCM ocean component uses the LANL Parallel Ocean Program (POP) model with a displaced North Pole over North America (Dukowicz and Smith 1994; Maltrud et al. 1998; Smith et al. 1995). The grid has an average resolution of 2/3° latitude and longitude with increased latitudinal resolution near the equator of approximately 1/2°. Two views of the horizontal grid structure of the ocean component are shown in Fig 1a, b. Because of the displaced pole, there is higher horizontal resolution in the eastern North Pacific, in the Arctic Straits near the northern Canada Archipelago, near Greenland, and in the Gulf Stream area. There is also special treatment given to the various straits and bottom topography to obtain the near observed ocean flow transports. Experience with a more conventional latitude-longitude grid structure in the Arctic region results in a poor ocean simulation, while the POP grid yields excellent Arctic Ocean flow patterns. Hudson Bay is not included or connected to the global ocean model due to the position of the displaced pole, but it is included as a non-dynamic "lake" in the land-surface model. The latitudinal resolution near the equator is enhanced in latitude down to 0.5 degrees. A narrow opening connects the Mediterranean and the Atlantic, which allows for a mixing of water between both oceans. The vertical diffusion parametrization in this version of the POP model makes use of the Pacanowski and Philander (1991) method which was originally designed for the tropical oceans. In its implementation here, the method mostly provides a minimum value of vertical mixing in the global ocean. Large et al. (1994) have developed a K-profile vertical parametrization scheme termed KPP. This newer scheme provides for more uniform mixing in the upper ocean

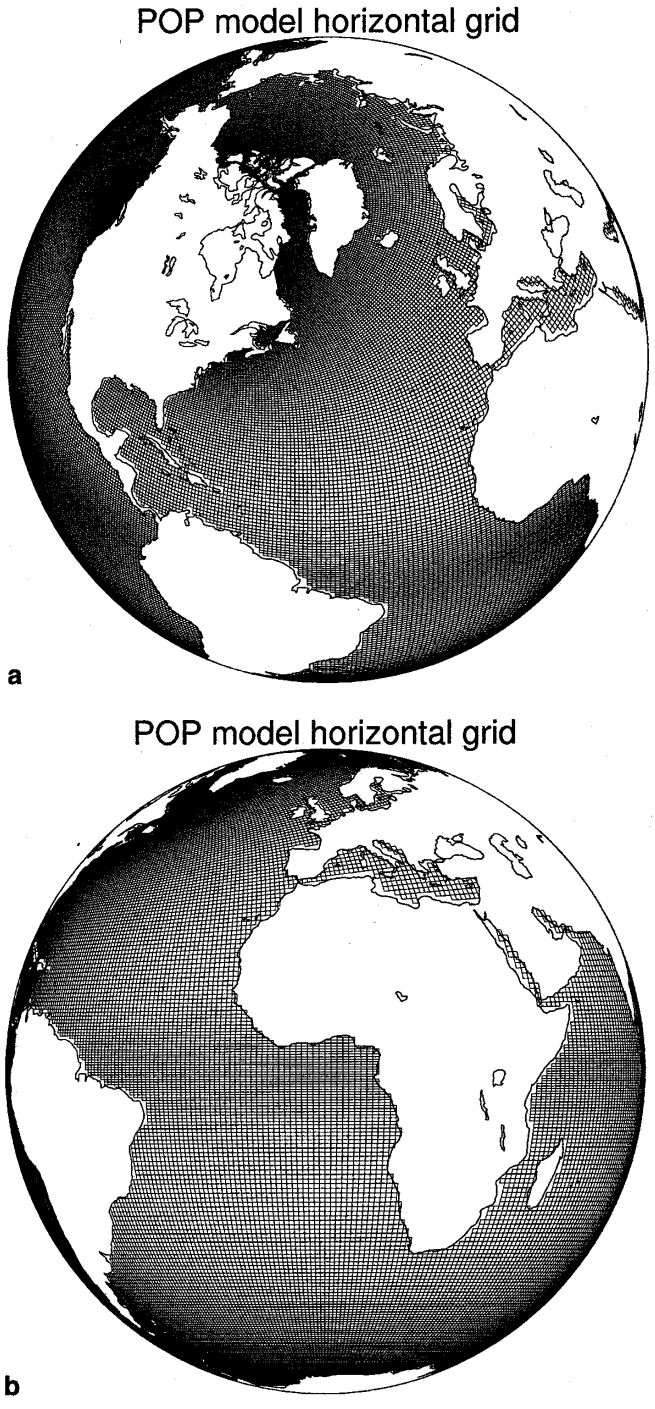


**Fig. 1a, b** Two views of the Parallel Ocean Program (POP) model horizontal grid at 2/3-degree resolution

and provides a good fit to the observations in a model with high upper ocean resolution and will be tested with future versions of the PCM. Visbeck et al. (1997) have devised a locally dependent version of Gent and McWilliams (1990) isopycnal mixing for the ocean component of the Hadley Centre climate model, which gives good results at a horizontal resolution of 2.25°. In future versions of the PCM, various forms of this isopycnal mixing will be tested.

While this version of PCM does not have an explicit river transport model, the mean observed annual estimate of river transport to the Arctic (3300 $km^3\ yr^{-1}$, Aagaard and Carmack, 1989) is prescribed as input to the Arctic Ocean. An estimate of the mean fresh water influx from Antarctic glacial calving and runoff ($8.4 \times 10^4\ m^3\ yr^{-1}$), although small, is included around Antarctica. The Arctic runoff has significant impact on the Arctic halocline, as well as on the strength of the overturning circulation in the North Atlantic (Weatherly and Washington 1999). The globally averaged water flux over the ocean-ice system (precipitation minus evaporation plus runoff) is set to zero, by scaling the local precipitation, to ensure conservation of global ocean salinity. Over the continental areas the total precipitation minus evaporation is added uniformly over the entire ocean without taking into account discharges from specific river basins. This is similar to what has been done for the CSM, although with slightly smaller effect due to the inclusion of the prescribed observed Arctic and Antarctic runoffs. These polar runoffs are uniformly added to the ocean along the coastlines. Marcia Branstetter and Jay Famiglietti of the University of Texas at Austin have implemented a parallel computer global river transport model component into later versions of the PCM. This component uses the technique developed by Miller et al. (1994). It will be used in future simulations of the PCM.

## 4 Sea-ice component

The sea-ice component is a fully dynamic-thermodynamic model, adapted from Zhang and Hibler (1997) of Naval Postgraduate School and optimized for MPP architecture by A. Craig of NCAR. It predicts the evolution of ice thickness, ice concentration, velocity, snow thickness, and surface temperature of ice (and snow-covered sea ice) in response to winds, ocean currents, air and ocean temperatures, humidity, radiation, and internal ice stresses. The sea-ice model also computes leads. The ice dynamics is the elastic-viscous-plastic (EVP) ice rheology of Hunke and Dukowicz (1997), which has been shown to produce similar results to the Zhang and Hibler (1997) viscous-plastic rheology at similar resolutions (see Hunke and Zhang 1999). The EVP model uses less computing time than the sea-ice version that uses the viscous plastic (VP) approximation (see Zhang and Hibler 1997). The thermodynamics uses the one-layer ice and snow thermodynamic scheme from Semtner (1976), with a single ice thickness per grid cell (versus more complex multiple thickness-category models). The ice model is run on a Cartesian grid in the two high-latitude regions, centered over each pole, with a constant 27 km resolution, thus avoiding the problem of convergence near the pole as on a latitude-longitude grid. Figure 2a, b shows the Northern and Southern Hemisphere 27 km horizontal grid structures for the sea-ice model.

## 5 The distributed flux coupler

The flux coupler concept was developed initially for the NCAR Climate System Model (see NCAR CSM Flux Coupler, Technical Note NCAR/TN-24+STR, May 1996), and was enhanced and adapted for PCM use on distributed memory computer architectures. Specifically, as shown in Fig. 3, the flux coupler is the connecting mechanism between the PCM components and facilitates the exchange or computation of information, including state variables and heat, water, and momentum fluxes. Because the horizontal grids are quite different between the component models, the Jones (1999) interpolation scheme is utilized to perform an area-preserving mapping of data. The flux coupler also scales fluxes as necessary to conserve the total global energy exchange between the components. Up-to-date development and computer performance information on the PCM can be found at http://www.cgd.ucar.edu/pcm/.

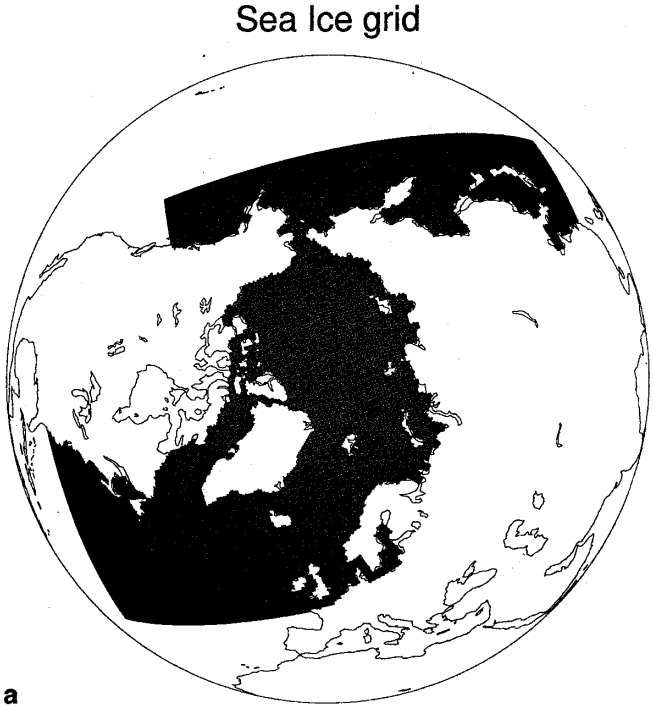


a

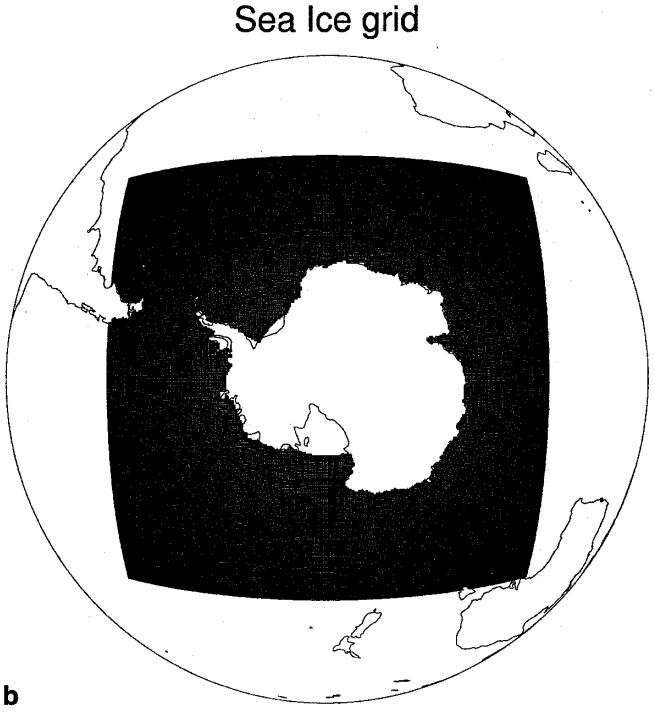


b

**Fig. 2a, b** Northern and Southern Hemisphere sea-ice grids at resolution of approximately 27 km

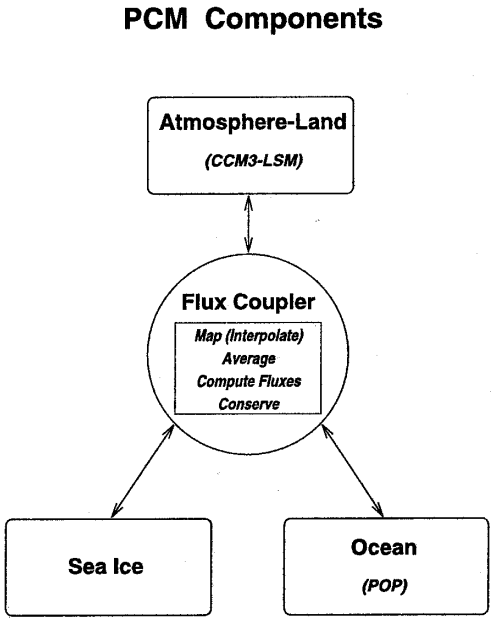


**Fig. 3** Schematic of the components of the PCM

## 6 PCM performance on parallel computers

The PCM utilizes a distributed memory programming paradigm method in the horizontal, which is incorporated using message passing. The original targeted computers were the distributed memory CRAY T3E-900 and the distributed shared memory SGI Origin 2000. While the PCM uses the CRAY shared memory access library (SHMEM) on the T3E, it has been modified to use the industry standard Message Passing Interface (MPI) library on the Origin. Thus, the PCM is portable and can be used on a variety of architectures from different computer vendors.

Generally speaking, the PCM scales relatively well from 16 to 64 processors on both machines. Using 64 processors, the PCM can complete a century long simulation in approximately one wallclock month. Presently, the PCM achieves a sustained performance of 2.6 Gflops on 64 processors on the Origin 2000, and 2.1 Gflops on 64 processors of the T3E.

Recently, the IBM RS/6000 SP parallel computer has become available for use with the PCM. The timing tests indicate comparable performance for 64 processors to the T3E and Origin systems. It should be kept in mind that many factors determine performance including processor speed, connection speeds between nodes, Fortran compilers, operating system, number of other executing programs on the computer, etc. Also, each machine requires some tuning of the model to take advantage of a particular computer system and its operating system software and library implementations.

## 7 Climate system initialization

In order to start up the coupled climate system, we use a spin-up strategy patterned after that of the CSM (Boville and Gent 1998). First, the atmosphere is integrated for 10 years with specified sea surface temperatures (Levitus 1982) and observed sea-ice concentrations. The 10-year time scale is required to allow the soil temperature and soil moisture to come into quasi-equilibrium with the atmosphere. The last five years of daily atmospheric output then

are used as the forcing for the ocean and sea-ice system. The ocean is first run with restoring to observed values of temperature and salinity. Then the ocean/sea-ice system is spun-up for 86 years with repeated five-year atmospheric forcing. The deeper ocean temperature and salinity fields are accelerated towards equilibrium by a factor of up to 10 as a function of depth using the technique of Bryan (1984). Although this technique does appear to help move the system closer to thermal equilibrium when the global ocean surface heat flux is near zero, it is clear that the subsurface ocean temperatures and salinities are not in equilibrium at the end of this spin-up due to the enormous thermal inertia and the time scale to change overall salinity by surface flux changes. It should be kept in mind that there are many sources of model errors in the treatment of atmospheric surface fluxes. For example, there are poorly understood processes such as cloud formulation and assignment of radiative forcing and boundary layer exchanges of heat, moisture, and momentum. Therefore, this initialization procedure cannot exactly reproduce observed fluxes. It does, however, provide an initial climate state that is compatible with the observed sea surface temperature distribution and tends to preserve it (with systematic errors noted below) in long-term simulations without any change in radiative forcing. In the fully coupled phase, the upper ocean and ice system shows small trends globally at the end of the initialization. The fully coupled model is then run for a 50-year adjustment period during which small changes were made to the background aerosol amount (from 0.14 to 0.08) to bring the global net surface flux imbalance from about $-1$ $Wm^{-2}$ to near zero at the end of this period. The fully coupled model is then run for three hundred years to establish the control experiment and several climate change experiments.

## 8 Control and climate change experiments

The globally averaged surface air temperatures for the control and 1% $CO_2$ increase per year climate change experiments are shown in Fig. 4. Specifically, the glob-

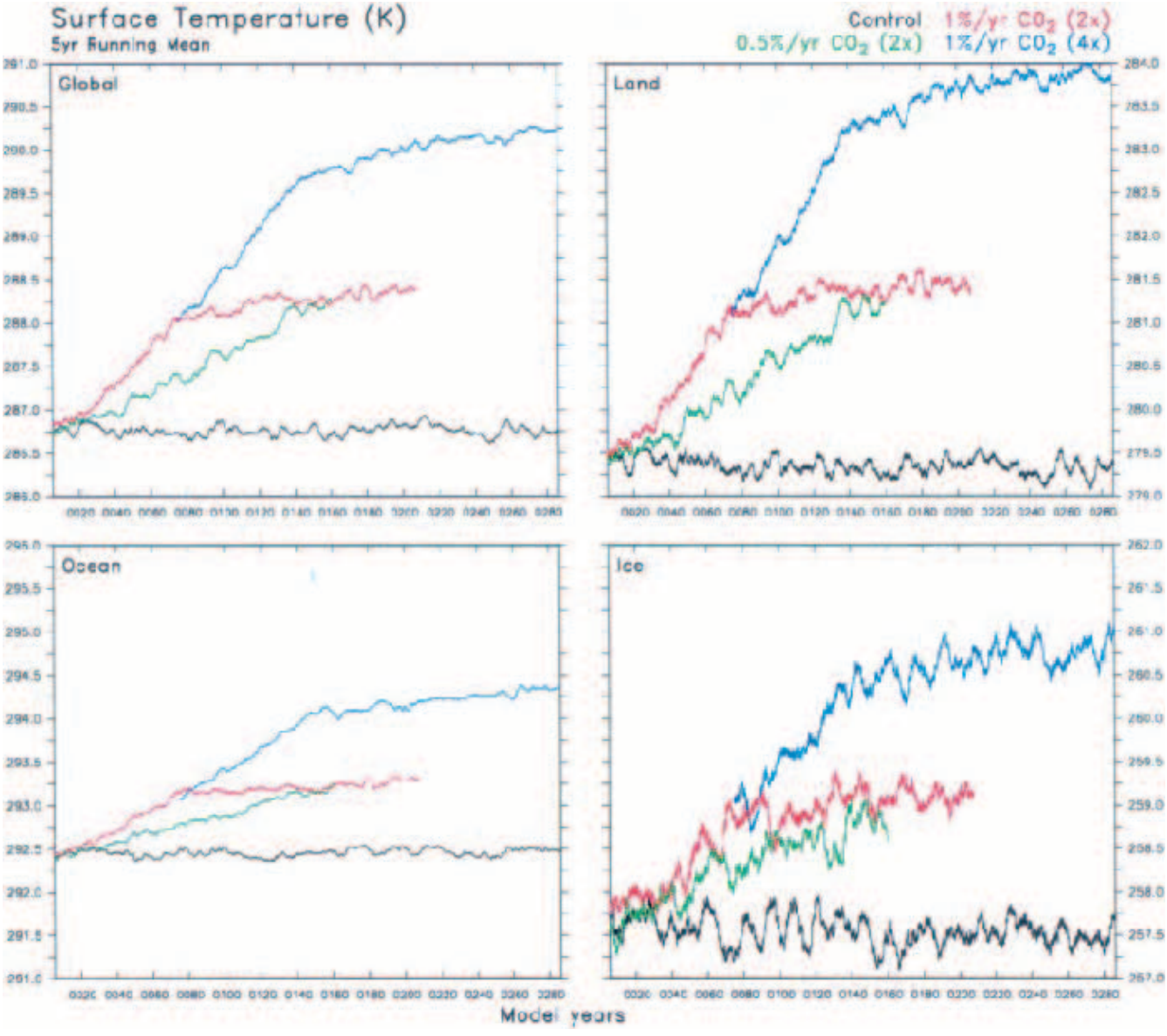


**Fig. 4a–d** Globally averaged surface temperature for control, transient, and instant sequestration simulations, **a** whole globe, **b** land area, **c** ocean area, and **d** sea-ice area. Note that the transient simulations have variants with $CO_2$ held constant after the doubling and quadrupling points

ally average surface temperature is shown as well as the globally averaged temperature over land, ocean, and sea ice. It should be pointed out that the areas of ocean surface and sea ice change slightly with time, which can affect the global numbers. Generally, over the last 250 years of the control simulation, the surface climate is stable with only a very small globally averaged temperature trend of 0.0174 °C per century. There are decadal time-scale oscillations in the ocean and sea ice plots. The transient experiment has a starting point $CO_2$ concentration of 355 PPM to doubling at 710 PPM near year 70. The global surface temperature warming for the 10 year average for years 66 to 75 at the doubling point is 1.27 °C, and for years 136–145 at the quadrupling point, the warming is 2.89 °C. The entire 300 year average of the control is used to compute the warming anomalies. The 0.5% $CO_2$ transient climate change experiment averaged for years 136–145 at the doubling point shows a warming of 1.49 °C.

The globally averaged sea surface temperature is shown in Fig. 5 and compared with the long-term mean of Levitus (1982), and National Centers for Environmental Predictions (NCEP) (see Kalnay et al. 1996) and from the long-term control average of CSM (see Boville and Gent 1998). Even though the atmospheric model component is the CCM (version 3.2), the ocean and sea-ice model are quite different, thus these changes can account for some of the differences with the CSM control simulation. Note also that surface temperature in the $2 \times CO_2$ stabilization experiment has only a small continuous warming trend after the capped doubling point. The $4 \times CO_2$ stabilization experiment has a larger warming rate for more than 50 years after capping at the $4 \times CO_2$ point. This is similar to what has been seen in other model experiments (e.g., Manabe and Stouffer 1993).

Figure 6 shows the time change of ocean temperature at various depths (12.6 m, 141 m, 519 m, 2280 m, 3476 m and 4975 m.) There are significant changes ranging from several tenths °C per century to lesser amounts in the deeper parts of the ocean. Note that the temperature scale is exaggerated to show the trends, which in the deeper levels of the ocean are quite small. By the end of the $2 \times CO_2$ and $4 \times CO_2$ experiments, the temperature drifts in the upper ocean (down to 141 m in Fig. 6b) have not leveled off; however, there is little trend in the control experiment near the top of the ocean. The control does show a trend at the 3476 m level. Because of the very large heat capacity of the ocean, it would take several thousand years for the entire depth of the ocean to come into equilibrium with the surface forcing from the atmosphere. In the observed climate system equilibrium can only be achieved if the heat and salinity fluxes at the top of the ocean are near zero for a time scale of the order of thousands of years.

The global sea-ice area for both hemispheres is shown in Fig. 7. In the control simulation, the hemispheric sea-ice area average shows very small trends; however, the sea-ice area average is either at or somewhat larger than observed maxima in both hemispheres. The sea ice in the Southern Hemisphere has an average

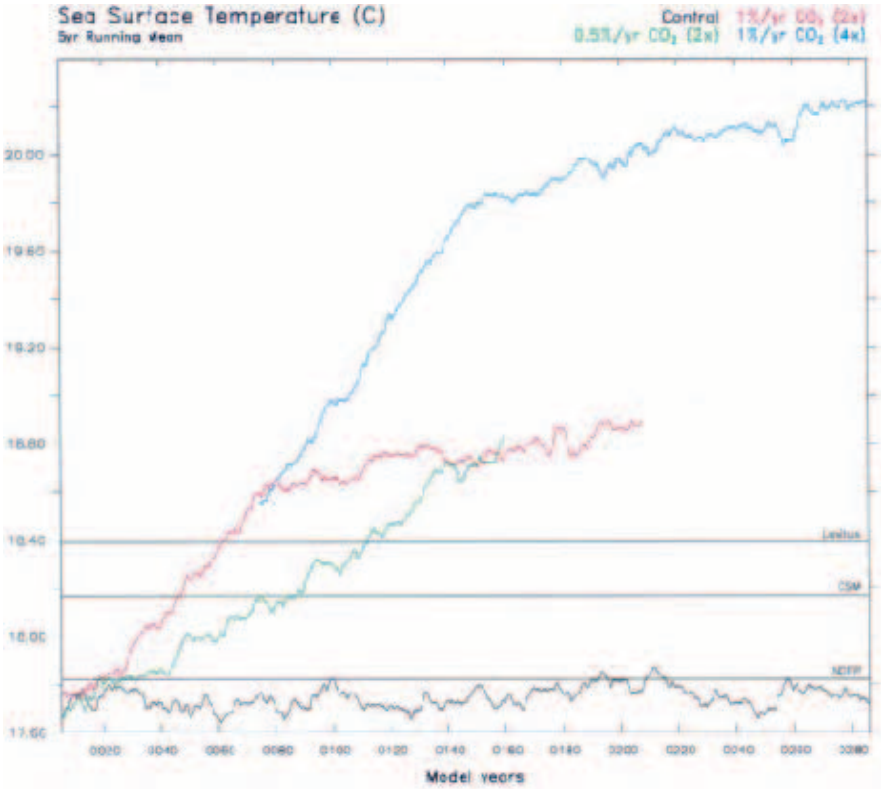


**Fig. 5** Globally averaged sea surface temperature for control, transient, and $2 \times CO_2$ and $4 \times CO_2$ stabilization simulations. Also, shown are the *Levitus*, and *NCEP* observed long-term means as well as the *CSM* (Boville and Gent 1998) simulation mean

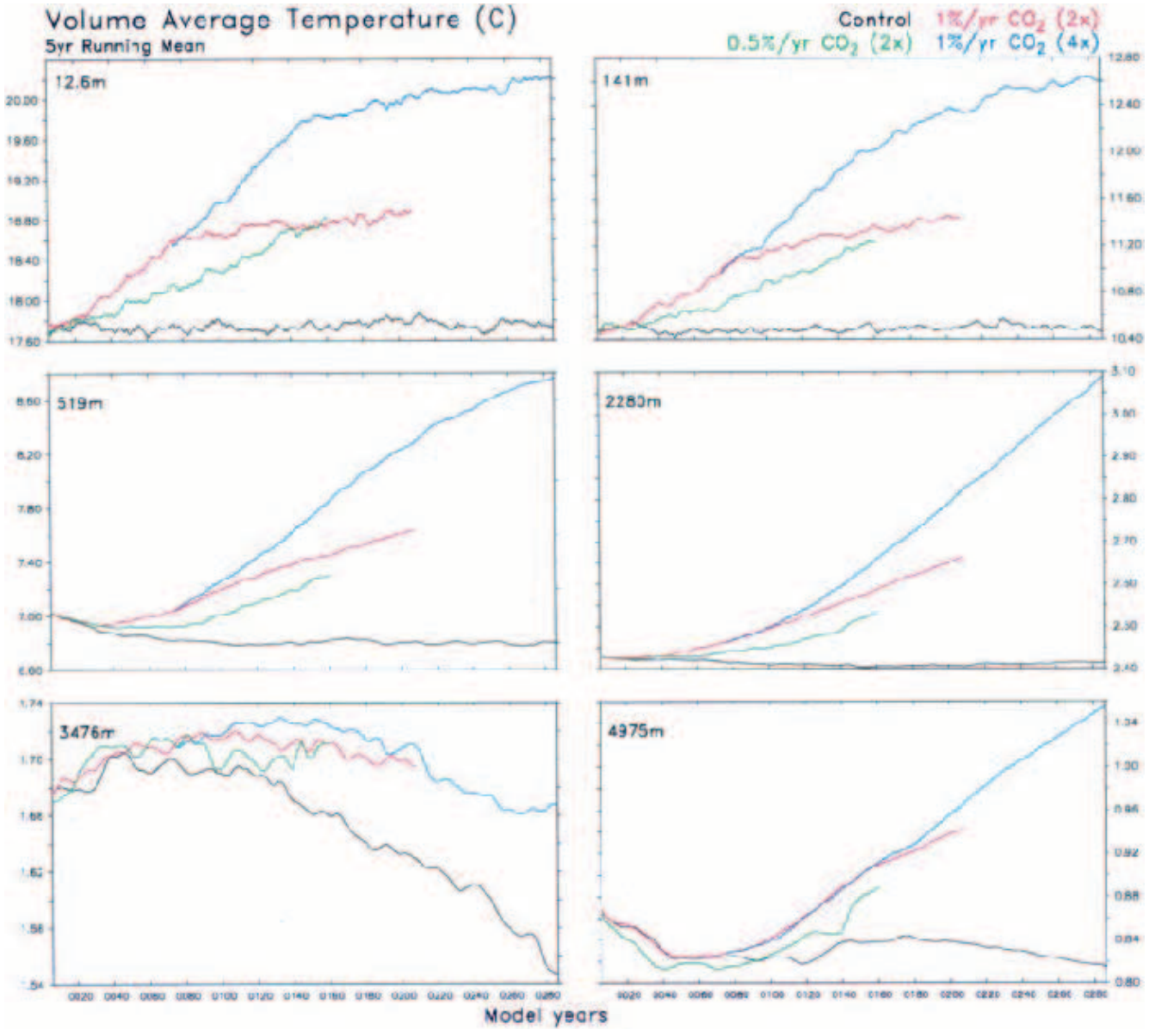


**Fig. 6** Globally averaged ocean temperature at various depths in meters for control, transient, and stabilization simulations

thickness of about 0.5 to 1 m; and for the Northern Hemisphere the average thickness is less than 2 m which is below observation-based estimates of 2.25 m. In the transient simulation at the doubling point of $CO_2$, the ice volume and area decrease substantially by about 10% to 30%, respectively, and 30% to 59% at the quadrupling point. Table 1 shows a more detailed breakdown of sea-ice area and volume change for the 1% transient at the doubling point, and the 0.5% transient at the doubling point. A more detailed analysis of the simulated sea ice is being prepared by Weatherly and Zhang (2000).

The time series of annual mean sea surface temperature in the Nino3 and Nino4 regions is shown in Fig. 8 for a 300-year period from the control integration and for the three 1% $CO_2$ increase per year climate change experiments. The amplitude of the El Niño/La Niña cycle in the PCM is close to the observed with the standard deviation of annual Nino3 sea surface temperatures from the PCM being 0.64 °C compared to the observed value (using the NCEP/NCAR Reanalyses from 1958–1998) of 0.66 °C. For the Nino4 region, the PCM standard deviation is 0.48 °C and the observed is 0.49 °C. Thus, the coupled climate model has about the observed amplitude of El Niño and La Niña events. A discussion of the reasons for the higher amplitude El Niño and La Niña cycles compared to previous model versions are discussed in Meehl et al. (2000b). That paper also shows the PCM simulates an east-west equatorial SST gradient in the equatorial Pacific that is close to the observed, but the PCM thermocline is more shallow than the observed. Examples of the tropical

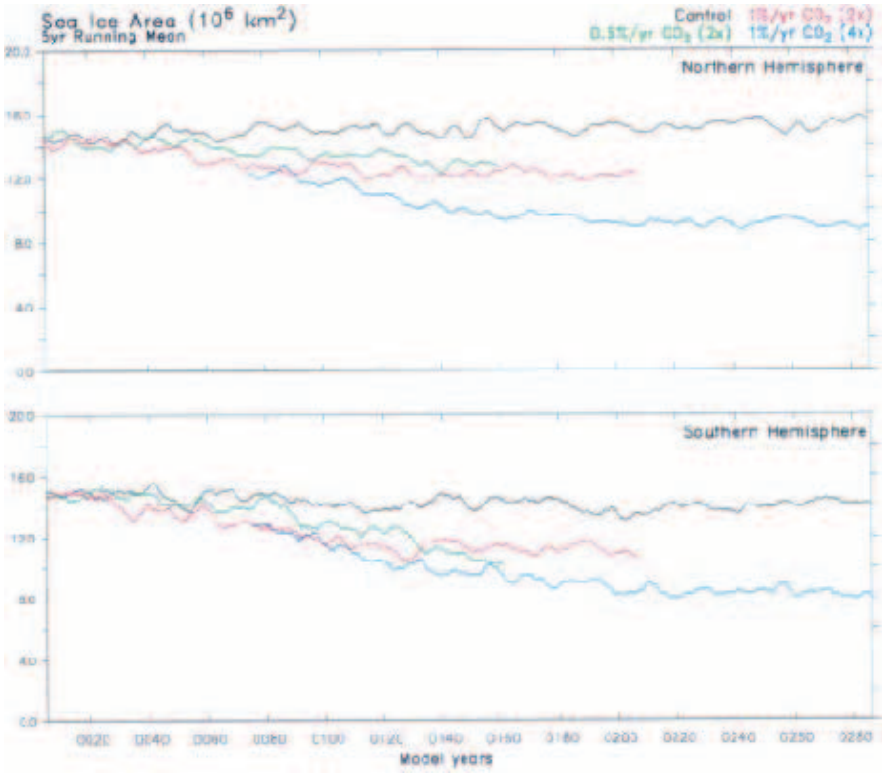


**Fig. 7** Hemispheric averages of sea-ice area ($10^6$ km$^2$)

**Table 1** Percentage differences in the hemispheric sea-ice area and volume for various experiments

| $2 \times CO_2$–control differences for the 1%/year $CO_2$ experiment | $2 \times CO_2$–control differences for 0.5%/year $CO_2$ experiment |
|---|---|
| NH area −13 | NH area −15 |
| SH area −12 | SH area −25 |
| NH volume −30 | NH volume −30 |
| SH volume −17 | SH volume −28 |

ocean aspects of the PCM are described in more detail in Semtner (1999).

To look at possible changes in El Niño amplitude or variability in climate change simulations, we computed the standard deviation of detrended Nino3 and Nino4 SSTs for the two $CO_2$ stabilization simulations and compared them to the control simulation. The $CO_2$ doubling and quadrupling stabilization experiments yielded standard deviation of 0.56 °C and 0.59 °C for Nino3 and 0.47 °C and 0.48 °C for Nino4 respectively which can be compared to 0.64 °C for Nino3 and 0.49 °C for Nino4 in the control run noted earlier. It is not clear that the lower standard deviations in the climate change simulations are significantly different from the control simulation.

The global distributions of surface temperature and sea level pressure patterns and their differences from observed for June–July–August (JJA) and December–January–February (DJF) ten-year averages are shown in Fig. 9a–c. The surface temperature and sea level pressure patterns in general are similar in pattern to the observed and the CSM results (Boville and Gent 1998; Boville and Hurrell 1998). For example, the major seasonal surface temperature and sea level pressure patterns between summer and winter are well simulated. The surface temperature differences (Fig. 9c) show the model is colder than observed, especially in the winter hemisphere. In the Southern Hemisphere the surface temperatures are too warm by several degrees mostly over the ocean areas.

The geographical difference plots in Fig. 10 of surface temperature and sea level pressure for the climate change experiments minus the control show patterns similar to those seen in previous climate change experiments. There is greater warming at high latitudes in the winter hemisphere than in the summer hemisphere that is mostly caused by the sea-ice albedo feedback and other effects such as changes in the low-level atmospheric lapse rate. Note the 0.5%/year experiment shows a very similar response to the 1% year experiment except it takes longer to get to the same $2 \times CO_2$ response.

The surface temperature differences in the tropical Pacific show little evidence of an El Niño-like pattern of mean climate change (Meehl and Washington 1996). The PCM uses the same atmospheric component as in the earlier version of the CSM, and that version of the CSM did not show evidence of an El Niño-like response pattern either (Meehl et al. 2000a). It was shown in that paper that cloud feedback related to cloud liquid water in the atmospheric model could contribute to the presence or absence of an El Niño-like response to increasing

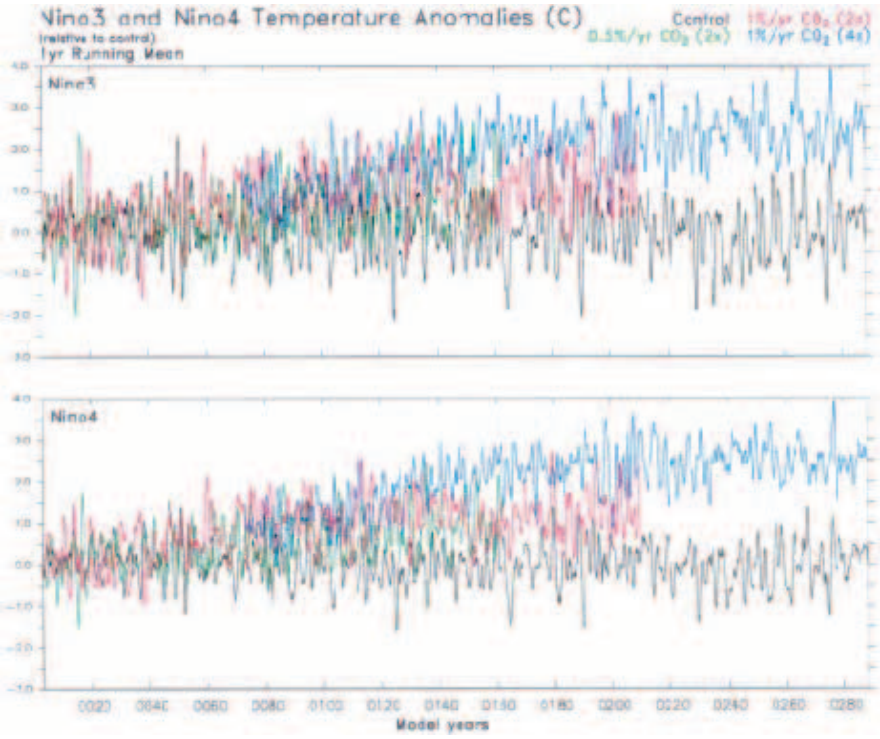


**Fig. 8a, b** Monthly mean time series of sea surface temperature anomalies for area-averaged **a** Nino3 (5°N–5°S, 90–150°W), **b** Nino4 (5°N–5°S, 160°W–150°W) with a one year running mean

$CO_2$ in a global coupled model. However, simply by uniformly warming the tropical Pacific, there are positive precipitation anomalies over that warmer water compared to the control experiment (not shown), and those precipitation anomalies are associated with a deepening of the Aleutian Low in the North Pacific (Meehl and Washington 1996) that is most notable in northern winter in DJF shown in Fig. 10. Similar patterns of temperature and sea level pressure change are seen for the $4 \times CO_2$ experiment in Fig. 10, but with much larger amplitude. Note the area of cooling in all three experiments south of Greenland, most notable in DJF, is associated with lower pressure in the North Atlantic and advection of relatively cooler air from North America.

## 9 Regional aspects of ocean and sea-ice simulations

The Arctic Ocean basin is usually simulated in climate models with a latitude-longitude grid structure and a pole point in the Arctic Ocean. This method can cause simulation difficulties due to the convergence of the meridians. Most modeling groups prefer not to use a shorter time step in that region. The most common techniques for dealing with the problem are to either smooth or Fourier filter the variables in that region along the longitudinal direction. This prevents an accurate simulation of the circulation in the Arctic basin. The POP model with displaced pole has effectively solved this problem for the near-surface Arctic Ocean currents shown in Fig. 11. There are no computational discontinuities in the vicinity of the North Pole. Several examples of the ocean circulation are shown in the following figures. Figure 12a, b shows instantaneous and long-term mean near surface current from the control simulation in the North Atlantic Basin, in which the Gulf Stream, the East Greenland Current and Labrador Current systems are well depicted. The instantaneous figure shows eddies in the 2/3° horizontal resolution and long-term mean shows the average current structure. Even such small features as the poleward surface current west of Spitsbergen is present. Flows in the Abyssal Basins and along the Central Arctic Lomonosov Ridge and flow through the Bering Strait are well simulated. These current systems bring heat to the northern polar region and are part of the worldwide ocean conveyor belt circulation. By the use of higher resolution ocean models, it is possible to more realistically capture the regional climate effects where, e.g., warm water can penetrate further north in models with finer resolution. Maltrud et al. (1998) and Smith et al. (2000) have shown that horizontal 1/6° and 1/10° grid spacings improve further the realistic aspects of the ocean system.

The annual mean Arctic sea-ice velocities from the control simulation and observed (Emery et al. 1998) are shown in Fig. 13. This figure shows the strong sea ice flow out of the Fram Strait. This is partly caused by a large central-Arctic anticyclone gyre, similar to that produced in CSM (Weatherly et al. 1998). There are eddy structures in many areas in the Arctic Basin in both sea ice and the ocean, although the sea ice has larger scale motion in

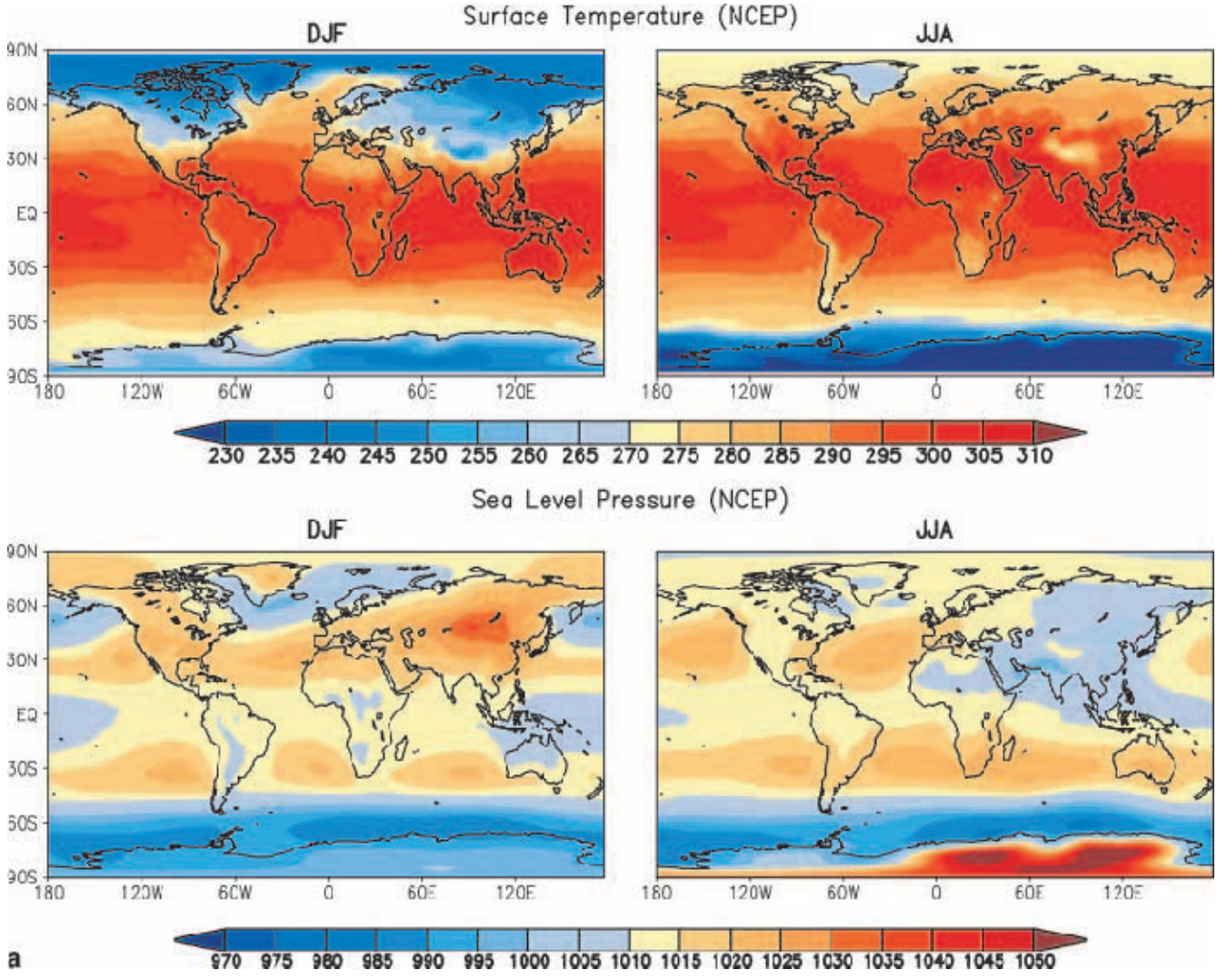


**Fig. 9a–c** Geographical NCEP distribution for December, January, and February (DJF) and June, July, August (JJA) surface temperature (*top*) control in K and sea level pressure (*bottom*) in mb in **a** The PCM control comparisons are shown in **b** The differences from observed are shown in **c**

response to wind forcing from synoptic weather systems. The surface ocean circulation also responds but seems to have an eddy structure that is smaller and, in places, quite independent of the motions of the sea ice. There are surface ocean and ice flows through parts of the Canadian Archipelago region, the McClure Strait and Nares Strait between Ellesmere Island and western Greenland. Because of the buildup of ice in Nares Strait, sea ice does not flow south in the winter season whereas ocean water under the sea does flow south. The PCM circulation patterns also appear to be consistent with the higher resolution study of Zhang et al. (1999) for the Arctic regions, however, the ocean eddies are weaker in this model because the resolution is coarser. There is an interesting question as to what should be the respective resolutions of sea ice and ocean components. The sea ice responds strongly to synoptic weather systems and the high-latitude ocean has smaller mesoscale eddies at higher latitudes due to the radius of deformation effect. We have chosen here to have the ocean resolution somewhat higher than the sea-ice model resolution to capture some of the effects of different scales in the ocean and sea-ice systems. With respect to the simulation capability in the Southern Hemisphere, we show in Fig. 14a, b the annual average sea-ice velocities around Antarctica from the model and those derived from satellite imagery (Emery et al. 1998). Note the strong westward flow adjacent to the coast of Antarctica is in agreement with the observations and the outward flow of sea ice from the Weddell and Ross Seas. Parkinson and Cavalieri (1989), Parkinson (1995) and Parkinson et al. (1999) and others have pointed out that the limited long-term observations of sea-ice changes show a large amount of regional and interannual variability. The most recent observations show decreasing sea-ice extents. Weatherly and Zhang (2000) have carried out a more detailed analysis of the sea-ice characteristics and compared them to recent and historical observations.

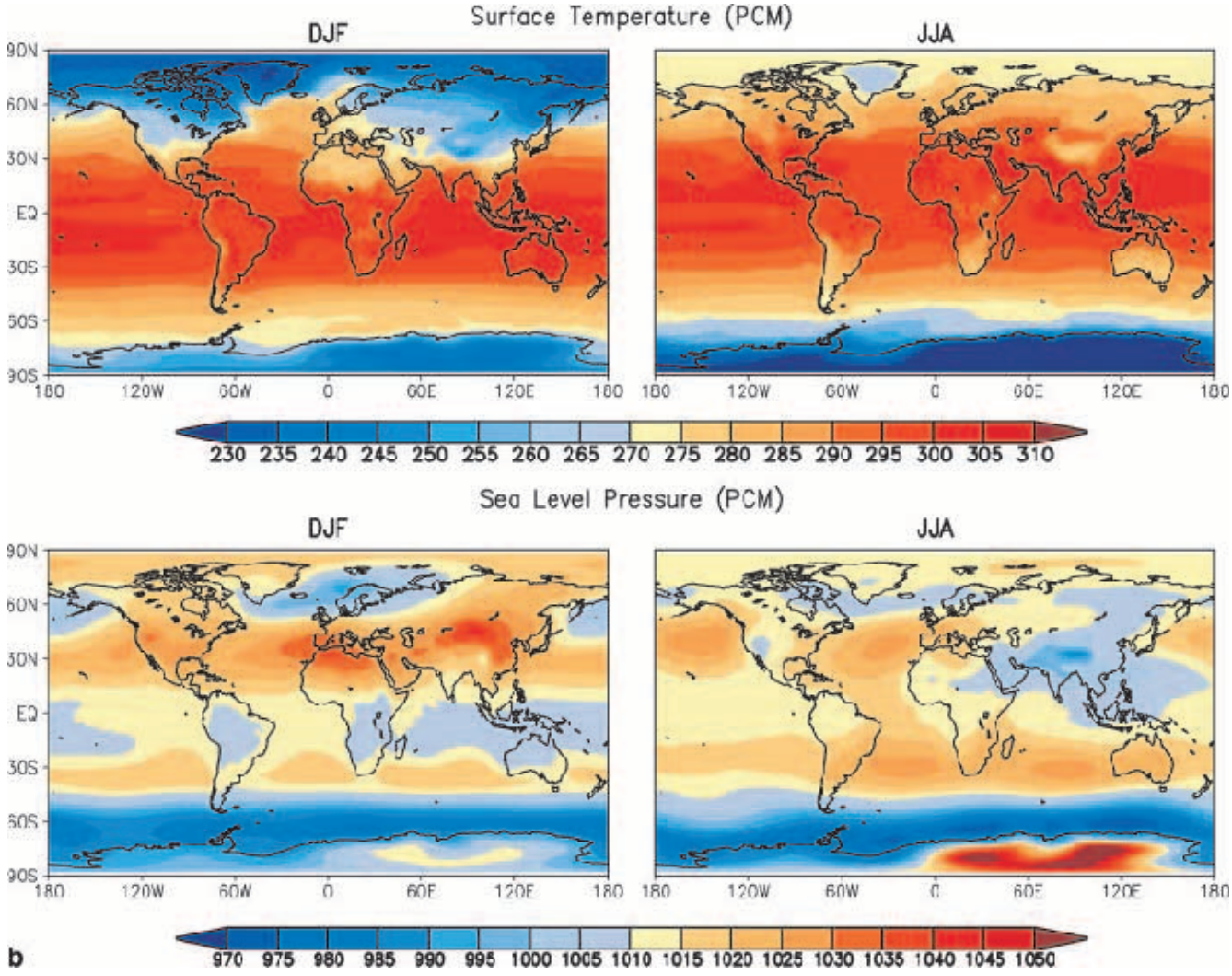


**Fig. 9** *Continued*

Bryan (1998) discusses in detail the heat transport in the CSM and the ramifications of lack of a river transport model for taking continental surface run-off to the oceans, and the precipitation-minus-evaporation balance used in CSM. Bryan (1998) found the excessive sea-ice production in the Southern Hemisphere in CSM, particularly in vicinity of the Ross and Weddell Seas, led to increased brine rejection, greater salinity, and overproduction of cold dense Antarctic Bottom Water (ABW). He also suggested the Antarctic Circumpolar Current (ACC) sped up in part due to redistribution of salinity caused by the excess northward sea ice transport. The increased sea-ice transport causes brine to form which, in turn, increases salinity as well as the north-south density gradient in the ACC region. The aerodynamic roughness length of sea ice was found to be too large in the CSM, was partly the cause of this problem and was subsequently corrected (Boville et al., 2000). Though this error is not in the OCM. We find similar behavior in PCM, with an excessively strong ACC (up to 270 Sv), and large northward sea-ice transport. However, in the PCM the lack of a Gent-McWilliams isopynical mixing formulation in the ACC region causes a too strong horizontal density gradient that in turn contributes to the ACC to be too strong. The addition of runoff from Antarctica does help to weaken the ACC but it is a small factor.

Figure 15 shows the global meridional overturning from the control and 1%/year $CO_2$ transient simulations. Because the displaced pole grid is used, the meridional overturning is computed along the model coordinates and then rotated to the north-south direction. The Northern Hemisphere meridional overturning maximum is about $30 \times 10^6$ m$^3$ s$^{-1}$ (1 SV = $10^6$ m$^3$ s$^{-1}$). Smith et al. (2000) has carried out a North Atlantic Ocean simulation with specified atmospheric forcing. That POP model has a horizontal resolution of 0.1°. Smith et al. (2000) found the N Atlantic meridional overturning to be 30 Sv similar in strength to that in the 2/3° model used in this study. The same is true with respect to horizontal heat transport in the North Atlantic (Fig. 16), where the maximum is near 1.2 Petawatts. Smith et al. (2000) also found the kinetic energy in the ocean eddies is larger in the higher resolution

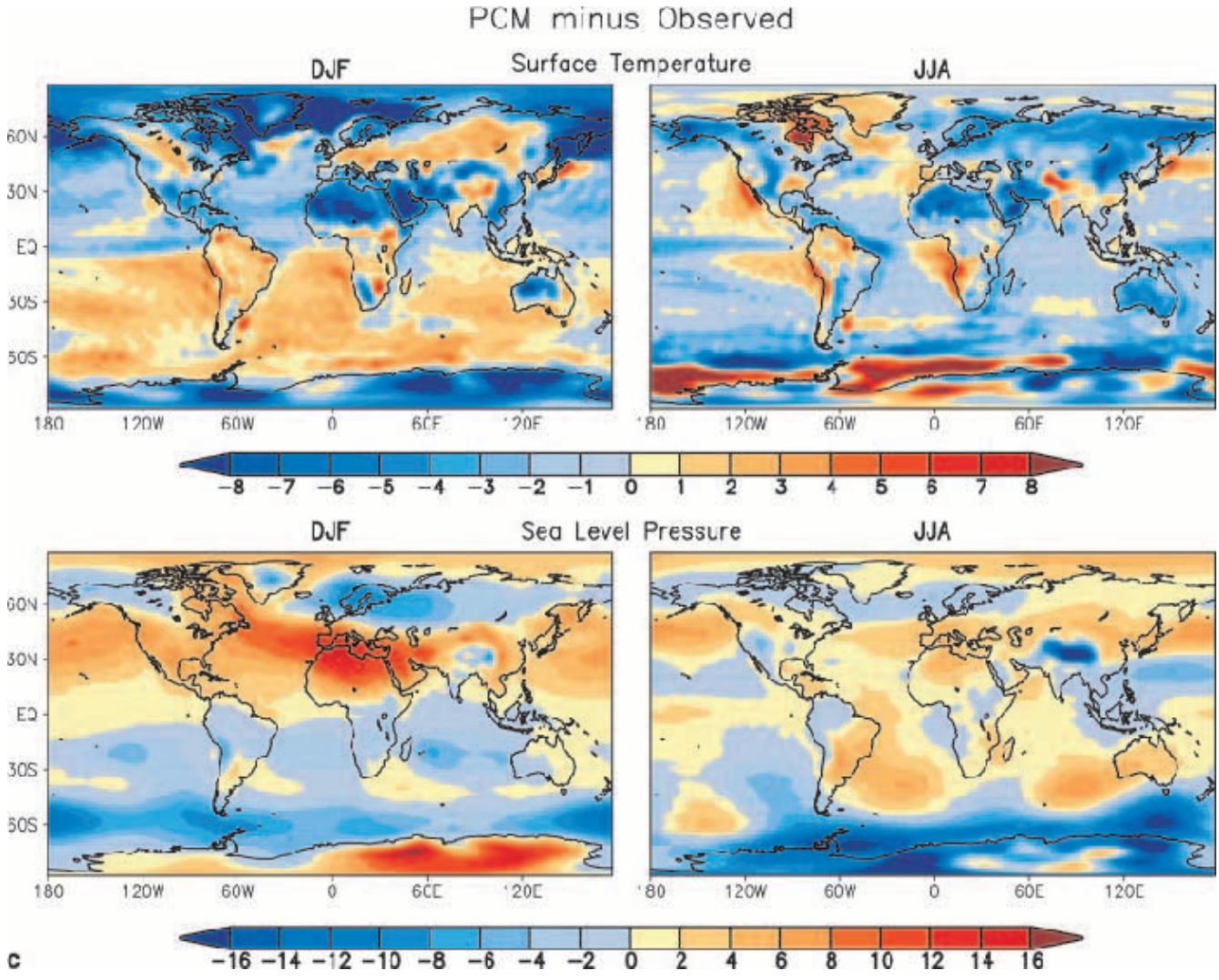


**Fig. 9** *Continued*

model simulations and that the current systems are closer to the observations. The coupled climate with 2/3° resolution ocean model yields a simulation of meridional overturning and horizontal heat transport that is close to the higher resolution models with specified atmospheric forcing. However, the PCM does not capture all of the details of a 0.1° ocean model. It should be pointed out that the ocean surface forcing fluxes of the standalone ocean model would be different than the fluxes of the coupled PCM simulation. In Fig. 15b, the 1%/year $CO_2$ transient simulation at the time of $CO_2$ doubling shows a weakening in the meridional overturning of around 10% from maxima of almost 30 Sv in the control to about 27 Sv.

The global horizontal heat transports for the control and 1%/year $CO_2$ at the doubling point of the transient simulation shown in Fig. 16 where the maximum at 15°N is nearly 2.7 Pw globally, and 1.3 Pw in the Atlantic (not shown but mentioned earlier). The transient run shows a reduction in the overall heat transport, which is consistent with the weakening of the meridional overturning changes in Fig. 15 and with previous climate model simulations of greenhouse gas warming. The change of heat transport near 40°S is due, in part, to upper ocean circulation of warm water around the southern part of Africa, which causes a local transport of heat towards the equator.

The PCM uses a free surface so sea level changes can be computed directly. In the 1%/year $CO_2$ transient experiments, the globally averaged sea level change at the time of $CO_2$ doubling is 7 cm, and 23 cm at quadrupling. The annual geographical mean distribution of sea level changes at the time of doubling and quadrupling are shown in Fig. 17. The sea level increase for the 0.5%/year $CO_2$ increase is greater than in the 1% integration at the time of doubling due to the longer time period taken to reach doubling in the 0.5% experiment which allows the ocean to absorb more heat through a deeper ocean depth. This is similar to that found by Stouffer and Manabe (1999). In terms of regional features; southeast of the Gulf Stream, the sea level has increased and to the northwest of the Gulf Stream, the

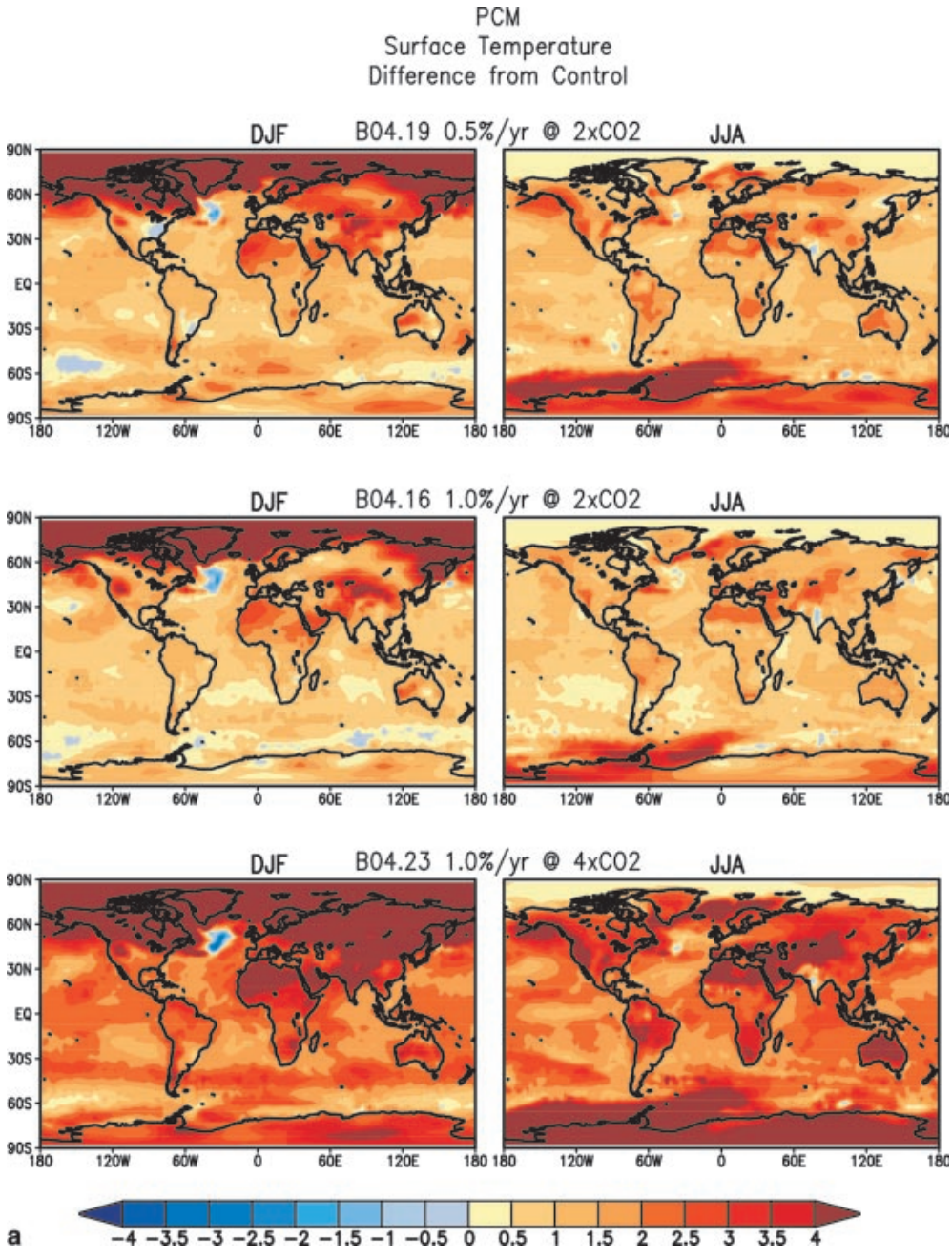


**Fig. 10** **a** Geographical distribution for December, January, and February (DJF) June, July, August (JJA) and December, January, February (DJF) surface temperature differences from control. (*Top*) 0.5%/year $CO_2$ transient at the doubling point, (*middle*) 1%/year $CO_2$ transient at the doubling point, (*bottom*) 1%/year $CO_2$ transient at the quadrupling point. Units are °C. **b** Similarly, the geographical distribution of DFJ and JJA sea level differences are shown for the respective experiments in mb

levels have lowered. This is consistent with the Gulf Stream position shifting more to the east and less penetration into the northern N Atlantic. Since the Gulf Stream is largely a geostrophic current the shift would result in an increase of sea level south of the current and lowering of sea level to the north of the Gulf Stream. This is mostly a dynamical effect from the slowing down of the conveyor belt circulation and is consistent with a weakening of the meridional overturning and poleward heat transport in the N Atlantic region as shown in Figs. 15 and 16. There are also shifts in the Labrador Sea region and a general lowering of sea level which is a result of the cooling of the ocean in this region as was discussed earlier as part of the strengthening of the Icelandic low pressure system. Positive differences near 45°S and negative differences to the south indicate a shift of the Antarctic circumpolar current towards the equator and slight strengthening. The sea level changes for the quadrupling $CO_2$ experiment show nearly the same pattern as the doubling but the changes are about twice the magnitude as shown in Fig. 16.

## 10 Summary

We have discussed the use of higher resolution ocean and sea-ice components with a new generation atmospheric model. Similar to previous coupled models

**Fig. 10** *Continued*

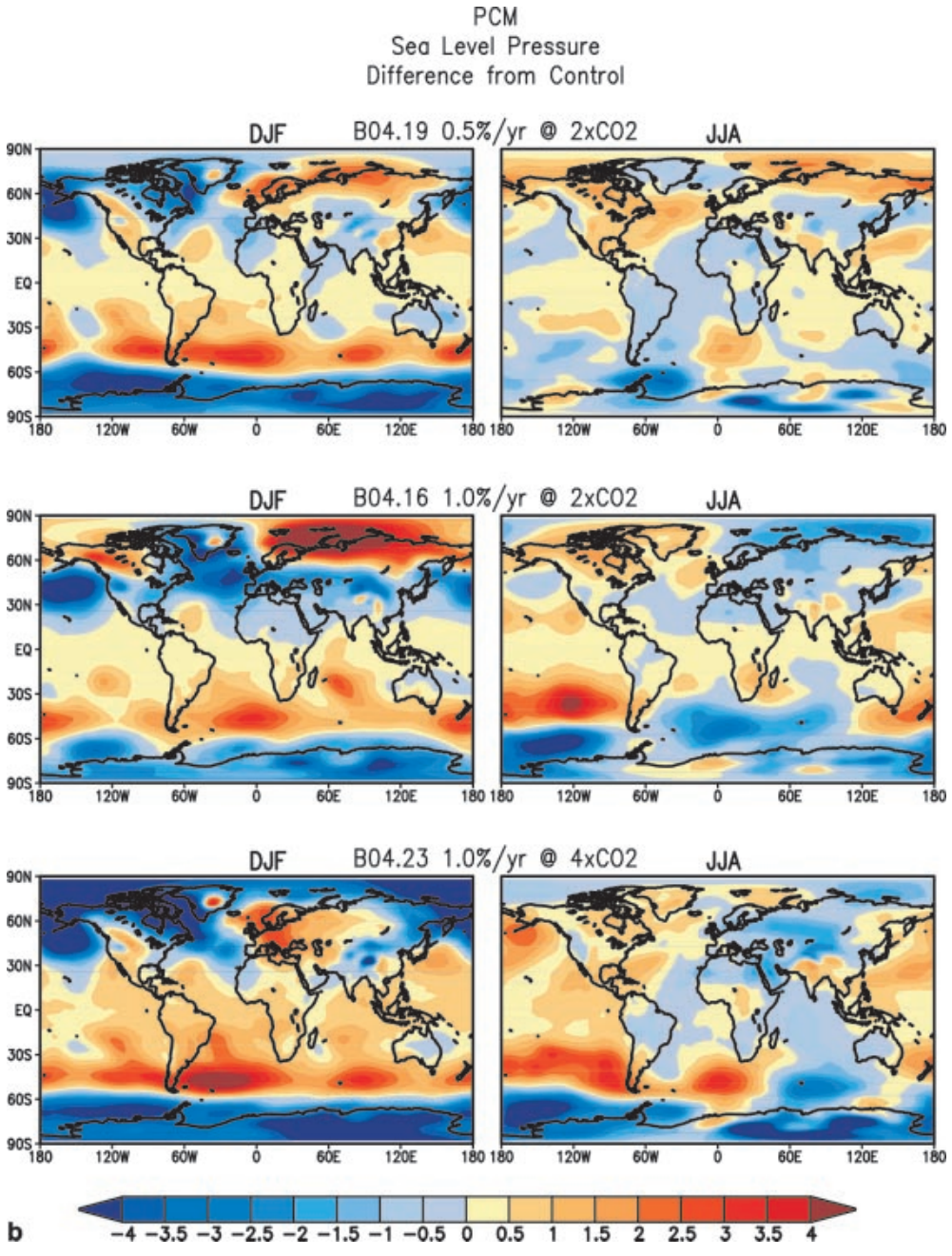


at NCAR, the PCM does not use a flux adjustment technique. The spin-up of the climate system makes use of observed sea surface temperatures to obtain atmospheric fluxes, which in turn are used to force the ocean and sea-ice system. This procedure provides an initial climatic state that is close to that where the observed ocean temperatures are specified. The surface climate has proved to be stable over a 300-year period of a control run simulating present-day climate. The global warming is 1.27 °C at the time of doubling and is 2.89 °C at the time of quadrupling for 1%/year increase of $CO_2$. For the 0.5%/year $CO_2$ increase experiment, the warming at the time of doubling is 1.5 °C. The regional patterns of climate change show greater warming at high latitudes in the winter hemisphere similar to that of other published simulations. The maximum warming is in the order of 8 °C in the Northern Hemisphere winter and 3–4 °C in the Southern Hemisphere winter mostly near the locations of sea-ice changes. There is little evidence of a long-term change in the averaged El Niño-like sea surface temperature response which is consistent with the version of the atmospheric model used in both the PCM and CSM (see Meehl et al. 2000a). The uniform warming of SSTs in the tropical Pacific is associated with positive precipitation anomalies there and a deepening of the Aleutian Low in winter. The patterns of surface temperature and sea level pressure change

are similar between the 1% $CO_2$ increase experiments at doubling and quadrupling. However, the 0.5% $CO_2$ increase experiment at doubling yields a somewhat different warming pattern and sea level change pattern due to the additional time allowed for the heat to penetrate into the ocean compared to the 1% $CO_2$ increase simulation. The ocean current and temperature patterns of the ocean are more realistic in both instantaneous and time mean patterns, particularly in many regional aspects. The amplitude of the El Niño cycle is close to observed, and is related to a sharper and shallower thermocline than in earlier simulations. The North Atlantic currents are closer to the observed than those found in ocean components of climate models of 2°–5° resolution. However, the areal coverage of sea ice is significantly greater than observed, and the Arctic ice motion pattern shows systematic bias, as forced by the atmospheric simulation. A new feature in the PCM is a free surface ocean formulation that allows direct calculation of sea level. Results from the doubling and quadrupling $CO_2$ experiments show 7 cm and 23 cm globally averaged sea level rise, respectively.

There are some new features that will be incorporated in the future versions of the PCM such as improvements to most of the major components. A parallel river transport model is being added for future experiments. Clearly, even on the decadal time scale the river runoff is a major factor on the ocean circulation. Presently, the PCM is being used for ensemble simulations of historical and future climate starting in 1870 and continuing to 2100. Greenhouse gases, stratospheric and tropospheric ozone, and effects of natural and manmade aerosols are included, as has also been done with the CSM (see Kiehl et al. 1999; Dai et al. 2000). Using the same climatic forcing will allow inter-comparison with the CSM and other scenario simulations.

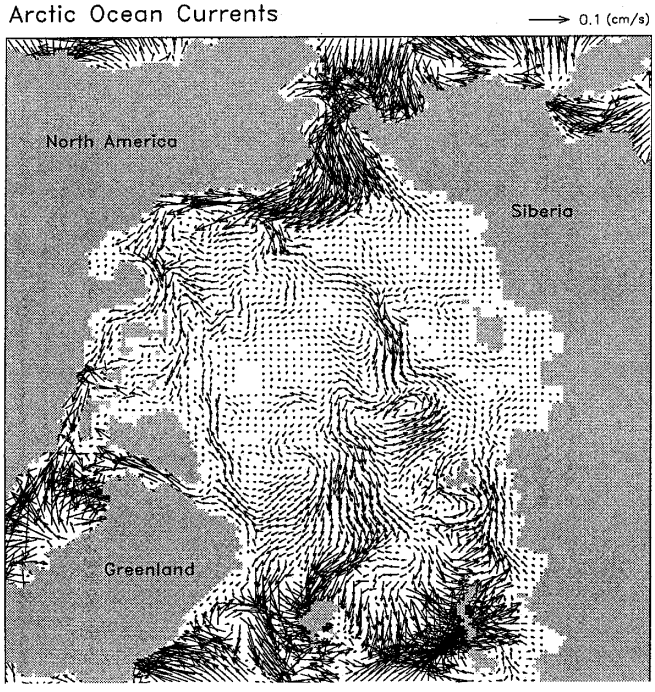


**Fig. 11a, b** Arctic Ocean upper ocean current velocity at a depth 37.9 m for January in the control simulation: **a** Instantaneous, **b** long-term mean

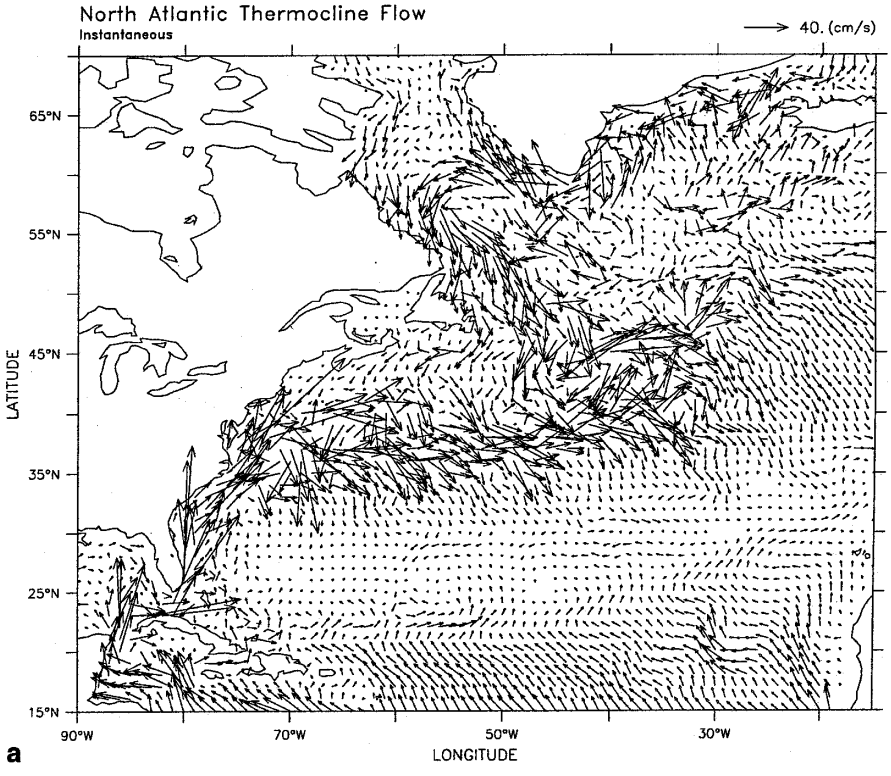


**Fig. 12** **a** Instantaneous and **b** time mean (5 years) North Atlantic top layer flow (25 m)

**Fig. 12** *Continued*

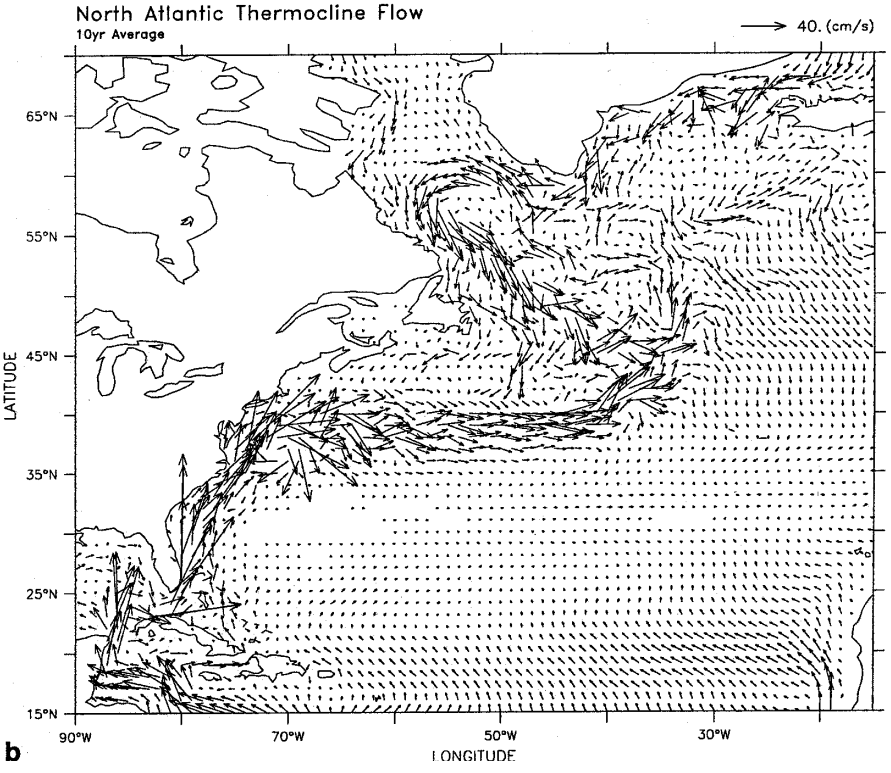


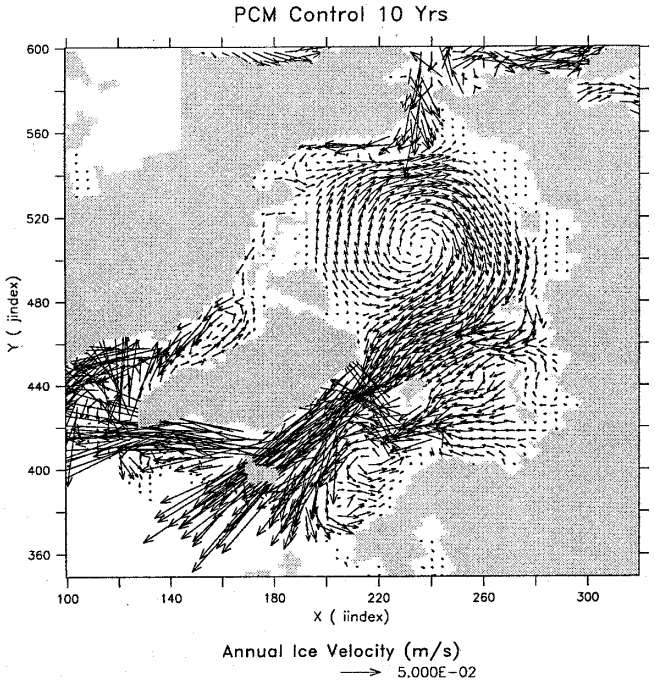


**Fig. 13** 10-year annual mean Arctic Ocean sea-ice velocities for the control run (scale vector 0.05 m $s^{-1}$, every 4th vector shown)

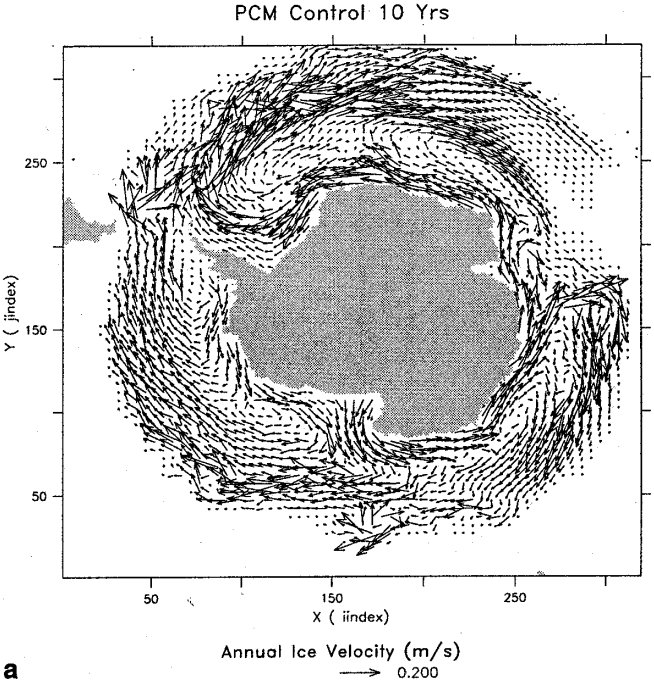


**Fig. 14 a** 10-year annual mean simulated sea-ice velocities for the Southern Hemisphere in the control run (scale vector 0.20 m $s^{-1}$, every 5th vector shown), **b** annual mean ice velocities derived from satellite date (Emery et al. 1998)

The PCM has been designed to make use of the new generation parallel computers that have a large number of nodes or clusters of processors. The Message Passing Interface (MPI) method has been effectively used to exchange data between nodes or within a node. The method of "open message passing" will be used in the future to pass infor-

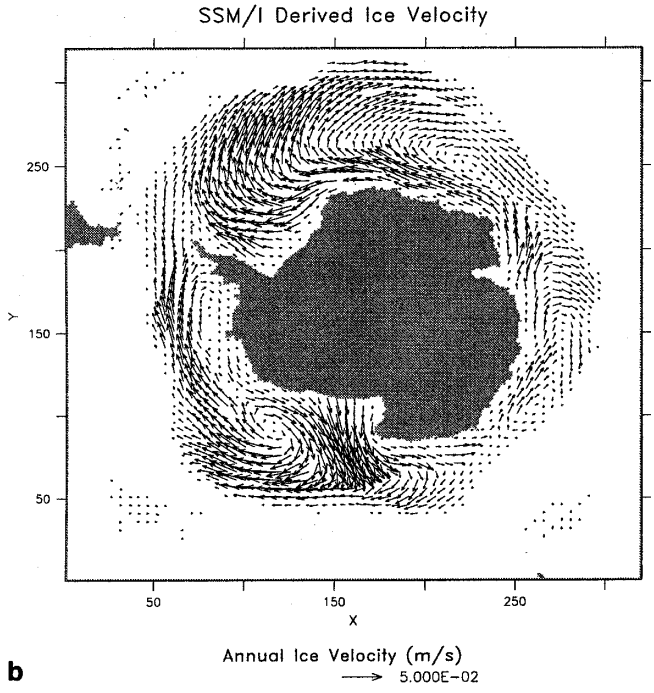


**Fig. 14** *Continued*

mation between processors within a node. The computational goal is to develop a state-of-art climate model that is capable of performing efficiently on large numbers of nodes and on a large number of processors within a node.

**Acknowledgements** The following are scientists and programming staff involved in the PCM effort or its components in alphabetical order: J. Arblaster (NCAR), T. Bettge (NCAR), A. Craig (NCAR), J. Dennis (NCAR), J. Dukowicz (LANL), J. Hack (NCAR), S. Hammond (NCAR), E. Hunke (LANL), R. James (NCAR), P. Jones (LANL), R. Loft (NCAR), R. Malone (LANL), M. Maltrud (LANL), W. Maslowski (NPS), G. Meehl (NCAR), A. Semtner (NPS), R. Smith (LANL), G. Strand (NCAR), W. Washington (NCAR), J. Weatherly (CRREL), V. Wayland (NCAR), D. Williamson (NCAR), and Y. Zhang (NPS).

The authors appreciate the involvement of R. Chervin in the early development of the PCM, especially the ocean component. The DOE CHAMMP and Climate Change Prediction Program (CCPP) and the National Science Foundation (NSF) support the research described. The computer time is being provided by the NCAR Climate Simulation Laboratory, the DOE National Energy Research Scientific Computing Center, and the Los Alamos National Laboratory's Advanced Computing Laboratory (ACL). Some of the graphics were generated by the use of the Ferret Graphics. The authors are very appreciative of the help in preparation of the manuscript by Stephanie Shearer. Several scientists from the Program for Climate Model Diagnosis and Intercomparison (PCMDI) such as Curtis Covey and Michael Wehner provided analysis of some of the results. David Pierce of the Scripps Institution of Oceanography also provided some insights as to the model performance in comparisons with climate observations. The reviewers provided the authors with many useful comments, which have been incorporated.

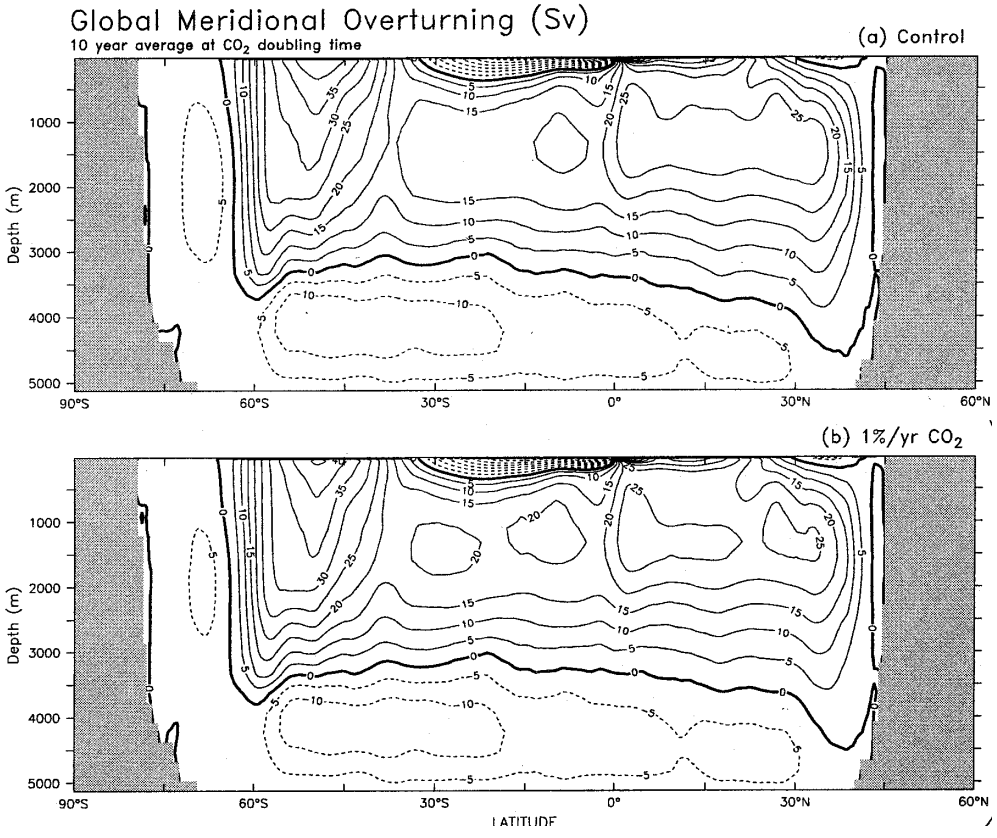


**Fig. 15a, b** Zonally averaged meridional overturning for the **a** control simulation and **b** transient simulation at the time of $CO_2$ doubling. Units are Sverdrups (1 Sv = $10^6$ m $s^{-2}$)

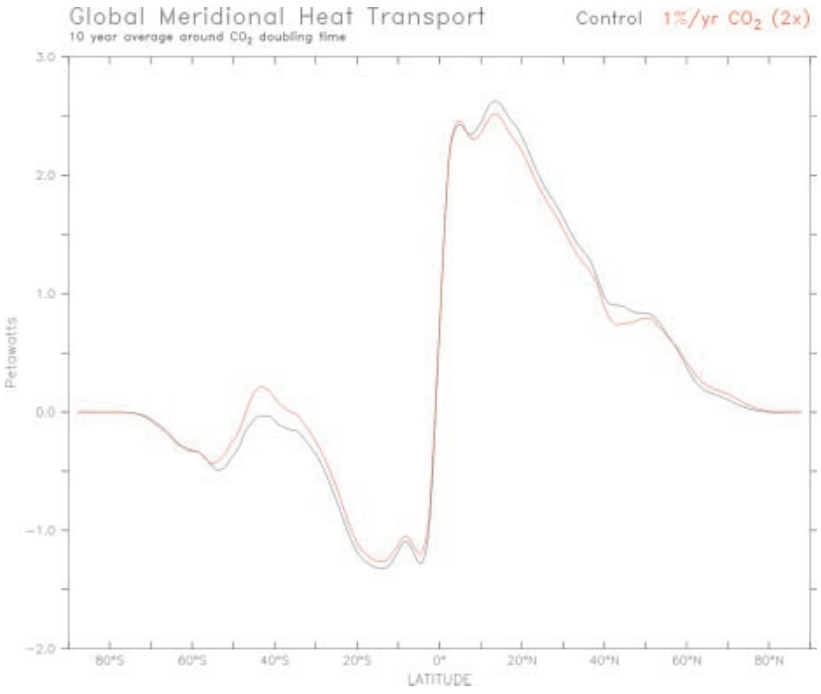


**Fig. 16** Zonally averaged global horizontal heat transport in the control simulation and transient simulation. Units are Petawatts

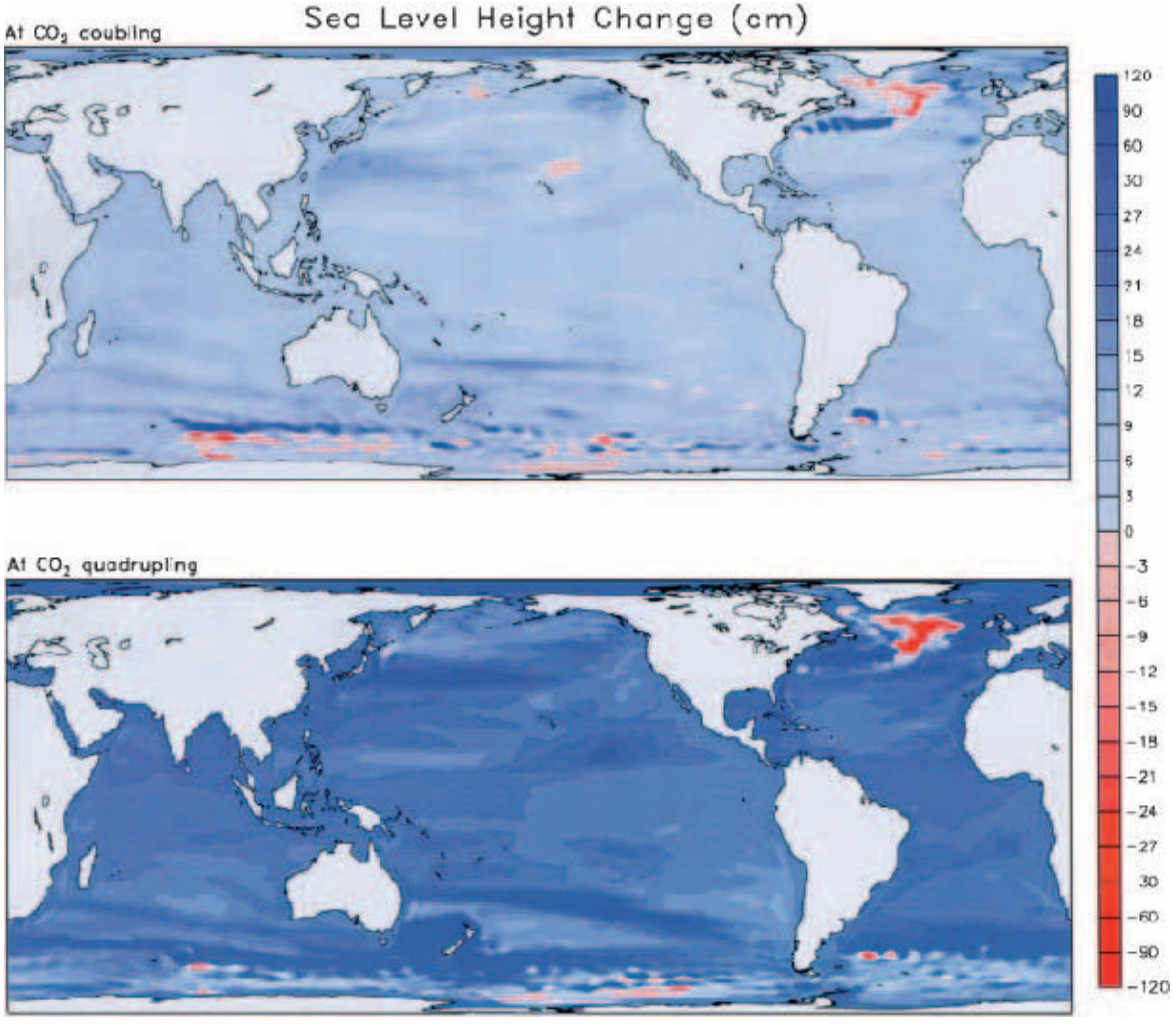


**Fig. 17** Geographical distribution of sea level change in cm for 1% $CO_2$ at the doubling point

## References


Aagaard K, Carmack EC (1989) The role of sea ice and other fresh water in the arctic circulation. J Geophys Res 94: 14 485–14 498

Bonan GB (1996) A land surface model (LSM version1) for ecological, hydrological, and atmospheric studies: technical description and user's guide. NCAR Technical Note NCAR/TN-417+STR. National Center for Atmospheric Research, Boulder, CO. 150 pp

Boville B, Gent PR (1998) The NCAR Climate System Model, version one. J Clim 11: 1270–1286

Boville B, Hurrell J (1998) A comparison of the atmospheric circulations in CCM3 and CSM1. J Clim 11: 1307–1326

Boville BA, Kiehl JT, Rasch PJ, Bryan FO (2000) Improvements to the NCAR CSM-1 for transient climate simulations. J Clim (in press)

Briegleb BP, Bromwich DH (1998) Polar radiation budgets of the NCAR CCM3. J Clim 11: 1246–1269

Bryan K (1984) Accelerating the convergence to equilibrium of ocean-climate models. J Phys Oceanogr 14: 666–673

Bryan FO (1998) Climate drift in a multicentury integration of the NCAR Climate System Model. J Clim 11: 1455–1471

Bryan FO, Kauffman BG, Large WG, Gent PR (1996) The NCAR CSM Flux Coupler. Technical Note, NCAR/TN-424+STR, NCAR, Boulder, CO

Dai A, Wigley TML, Boville BA, Kiehl JT, Buja L (2000) Climates of the 20th and 21st centuries simulated by the NCAR Climate System Model (CSM). J Climate (in press)

Drake J, Foster I, Michalakes J, Toonen B, Worley P (1995) Design and performance of a scalable parallel community climate model. Parallel Comput 21: 1571–1591

Dukowicz JK, Smith RD (1994) Implicit free-surface method for the Bryan-Cox-Semtner Ocean model. J Geophys Res 99: 7991–8014

Emery WJ, Fowler CW, Maslanik JA (1998) Satellite-derived maps of Arctic and Antarctic sea-ice motion. Geophys Res Lett 24: 897–900

Gent PR, McWilliams JC (1990) Isopycnal mixing in ocean circulation models. J Phys Oceanogr 20: 150–155

Hack JJ (1994) Parametrization of moist convection in the NCAR Community Climate Model (CCM2). J Geophys Res 99: 5551–5568

Hack JJ, Rosinski JM, Williamson DL, Boville BA, Truesdale JE (1995) Computational Design of the NCAR community climate model. Parallel Comput 21: 1545–1569

Holtslag AAM, Boville BA (1993) Local versus non-local boundary layer diffusion in a global climate model. J Clim 6: 1825–1842

Hunke EC, Dukowicz JK (1997) An elastic-viscous-plastic model for sea ice dynamics. J Phys Oceanogr 27: 1849–1867

Hunke EC, Zhang Y (1999) A comparison of sea ice dynamics models at high resolution. Mon Weather Rev 127: 396–408

Hurrell J, Hack JJ, Boville BA, Williamson D, Kiehl JT (1998) The dynamical simulation of the NCAR Community Climate Model version 3 (CCM3). J Clim 11: 1207–1236

Intergovernmental Panel on Climate Change (IPCC) (1996) Climate change 1995: IPCC Second Assessment Report. Cambridge University Press, Cambridge, UK, pp 572

Jones P (1999) First and second-order conservative remapping. Mon Weather Rev 127: 2204–2210

Jones PD, New N, Parker DE, Martin J, Rigor IG (1999) Surface air temperature and its changes over the past 150 years. Rev Geophys (in press)

Kalnay E, coauthors (1996) The NCEP/NCAR 40-year reanalysis project. Bull Am Meteorol Soc 77: 437–471

Kiehl JT, Hack JJ, Bonan GB, Boville BA, Williamson DL, Rasch PJ (1998) The National Center for Atmospheric Research Community Climate Model: CCM3. J Clim 11: 1131–1149

Large WG, McWilliams JC, Doney SC (1994) Oceanic vertical mixing: a review and a model with a nonlocal boundary layer parametrization. Rev Geophys 32: 363–403

Levitus S (1982) Climatological Atlas of the World Ocean. NOAA Prof Pa 13, US Government Printing Office, Washington, DC, pp 173

Maltrud ME, Smith RD, Semtner AJ, Malone RC (1998) Global eddy-resolving ocean simulations driven by 1985–1995 atmospheric winds. J Geophys Res 103: 30 825–30 853

Manabe S, Stouffer RJ (1993) Century-scale effects of increased atmospheric $CO_2$ on the ocean-atmosphere system. Nature 364: 215–218

Meehl GA, Washington WM (1996) El Niño-like climate change in a model with increased atmospheric $CO_2$ concentrations. Nature 382: 56–60

Meehl GA, Arblaster J (1998) The Asian-Australian monsoon and El Nino-Southern Oscillation in the NCAR Climate System Model. J Clim 11: 1356–1385

Meehl GA, Collins W, Boville B, Kiehl JT, Wigley TML, Arblaster JM (2000a) Response of the NCAR Climate System Model to increased $CO_2$ and the role of physical processes. J Clim 13: 1879–1898

Meehl GA, Gent P, Arblaster JM, Otto-Bliesner B, Brady E, Craig A (2000b) Factors that affect the amplitude of El Niño in global coupled climate models. Clim Dyn, in press

Miller JR, Russell GL, Caliri G (1994) Continental-scale river flow in climate models. J Clim 7: 914–928

Pacanowski RC, Philander SGH (1981) Parametrization of vertical mixing in numerical models of the tropical oceans. J Phys Oceanogr 11: 1443–1451

Parkinson CL (1995) Recent sea-ice advances in Baffin Bay/Davis Strait and retreats in the Bellingshausen Sea. Ann Glaciol 21: 348–352

Parkinson CL, Cavalieri DJ (1989) Arctic sea ice 1073–1987: Seasonal, regional, and interannual variability. J Geophys Res 94(C10): 14 499–14 523

Parkinson CL, Washington WM (1979) A large-scale numerical model of sea ice. J Geophys Res 84: 311–337

Parkinson CL, Cavalieri DJ, Gloersen P, Zwally HJ, Comiso JS (1999) Arctic sea extents, areas, and trends, 1978–1996. J Geophys Res 104(C9): 20 837–20 856

Reynolds RW, Smith TM (1994) Improved global sea surface temperature analyses using optimum interpolation. J Clim 7: 929–948

Semtner AJ (1976) A model for the thermodynamic growth of sea ice in numerical investigations of climate. J Phys Oceanogr 6: 379–389

Semtner AJ (2000) Ocean and climate modeling on advanced parallel computers: progress and prospects, Communications of the ACM 43: 81–89

Smith RD, Maltrud ME, Bryan FO, Hecht MW (2000) Numerical simulation of the North Atlantic Ocean at 1/10 degree. J Phys Oceanogr 30: 1532–1561

Smith RD, Kortas S, Meltz B (1995) Curvilinear coordinates for global ocean models, LA-UR-95-1146, Los Alamos National Laboratory, Los Alamos, New Mexico, 38 pp

Stouffer RJ, Manabe S (1999) Response of a coupled ocean-atmosphere model to increasing atmospheric carbon dioxide: sensitivity to the rate of increase. J Clim 12(8): 2224–2237

Visbeck M, Marshall J, Haine T, Spall M (1997) On the specification of eddy transfer coefficients in coarse resolution ocean circulation models. J Phys Oceanogr 27: 381–402

Weatherly JW, Washington WM (1999) Arctic and Antarctic influences on thermohaline circulation in a global climate model. Fifth Conf Polar Meteorology and Oceanography (Preprints), 10–15 January 1999, Dallas, Texas, American Meteorological Society

Weatherly JW, Zhang Y (2000) The response of the polar climate to increasing $CO_2$ in a global climate model with elastic-viscous-plastic sea ice. J Clim (in press)

Weatherly JW, Briegleb BP, Large WG, Maslanik JA (1998) Sea ice and polar climate in the NCAR CSM. J Clim 11: 1472–1486

Zhang GJ, McFarlane NA (1995) Sensitivity of climate simulations to the parameterization of cumulus convection in the Canadian Climate Centre general circulation model. Atmos-Ocean 33: 407–446

Zhang JL, Hibler III WD (1997) On an efficient numerical method for modeling sea ice dynamics. J Geophys Res 102: 8691–8702

Zhang Y, Maslowski W, Semtner AJ (1999) Impacts of mesoscale ocean currents on sea ice in high-resolution Arctic ice and ocean simulations. J Geophys Res 104: 18 409–18 429